Myoconductive and osteoinductive free-standing polysaccharide membranes

Sofia G. Caridade, Claire Monge, Jorge Almodóvar, Raphaël Guillot, Jonathan Lavaud, Véronique Josserand, Jean-Luc Coll, João Mano, Catherine Picart

Published in final edited form as:
Acta Biomater. 2015 March ; 15: 139–149. doi:10.1016/j.actbio.2014.12.027.

Myo-conductive and osteo-inductive free-standing polysaccharide membranes

Sofia G. Caridade[1,2,3,#], **Claire Monge**[3,4,#], **Jorge Almodóvar**[3,4,†], **Raphael Guillot**[3,4], **Jonathan Lavaud**[5], **Véronique Josserand**[5], **Jean-Luc Coll**[5], **João F. Mano**[1,2], and **Catherine Picart**[3,4]

[1]3B's Research Group – Biomaterials, Biodegradables and Biomimetics, University of Minho, Headquarters of the European Institute of Excellence on Tissue Engineering and Regenerative Medicine, AvePark, Zona Industrial da Gandra, S. Cláudio do Barco, 4806-909 Caldas das Taipas – Guimarães, Portugal.

[2]ICVS/3B's - PT Government Associate Laboratory, Braga/Guimarães, Portugal

[3]CNRS, UMR 5628, LMGP, 3 parvis Louis Néel, F-38016 Grenoble, France

[4]Université de Grenoble Alpes, Grenoble Institute of Technology, 3 parvis Louis Néel, F-38016, Grenoble, France.

[5]Institute Albert Bonniot, INSERM U823, ERL CNRS3148, Grenoble, France

Abstract

Free-standing (FS) membranes have increasing applications in the biomedical field as drug delivery systems for wound healing and tissue engineering. Here, we studied the potential of free-standing membranes made by the layer-by-layer assembly of chitosan and alginate to be used as a simple biomimetic system of the periosteum. The design of a periosteum-like membrane implies the elaboration of a thick membrane suitable for both muscle and bone formation. Our aim was to produce well defined ~50 μm thick polysaccharide membranes that could be easily manipulated, be mechanically resistant, and enable both myogenesis and osteogenesis *in vitro* and *in vivo*. The membranes were chemically crosslinked to improve their mechanical properties. Crosslinking chemistry was followed via FTIR and the mechanical properties of the membranes were assessed using dynamic mechanical analysis. The loading and release of the potent osteoinductive growth factor bone morphogenetic protein 2 (BMP-2) inside and outside of the FS membrane was followed by fluorescence spectroscopy in a physiological buffer over one month. The myogenic and osteogenic potential of the membranes *in vitro* was assessed using BMP-2 responsive skeletal myoblasts. Finally, their osteoinductive properties *in vivo* were studied in a preliminary experiment using a mouse ectopic model. Our results showed that the more crosslinked FS membranes enabled a more efficient myoblast differentiation in myotubes. In addition, we showed that a tunable amount of BMP-2 can be loaded in and subsequently released from the membranes depending on the crosslinking degree and BMP-2 initial concentration in solution. Only the more

Corresponding authors: catherine.picart@grenoble-inp.fr, phone: +33(0)4 56 52 93 11, fax: +33(0)4 56 52 93 01. jmano@dep.uminho.pt, phone: +35 12 53 51 09 00, fax: +35 12 53 51 09 09.
[†]Current address: University of Puerto-Mayagüez, Department of Chemical Engineering, PO Box 9000, PR 00681-9000, Puerto Rico.
[#] co-first authors; these authors contributed equally

Europe PMC Funders Author Manuscripts

crosslinked membranes were found to be osteoinductive *in vivo*. These polysaccharide-based membranes have strong potential as a periosteum-mimetic scaffold for bone tissue regeneration.

Keywords

Polysaccharides; layer-by-layer; biomaterials; tissue engineering; free-standing membranes; dynamic mechanical analysis; muscle; bone; osteoinduction

Introduction

Bone structure is characterized as a 3D complex tissue composed of cells and mineralized extracellular matrix (ECM). Ongoing research in the field of biomaterials aims to better mimic the properties of natural tissues [1] and to guide cell fate locally for regenerating damaged tissues [2]. There are several membrane-like native tissues, which have important physiological roles. For instance, the periosteum—or pericranium for the skull—is a thick membrane covering the outer surface of all bones except of sites of articulation [3]. It consists of an outer fibrillar layer and an inner cellular layer, whose thickness varies according to age and species (eg 40 μm in mouse tibiae [4], 100 μm for human tibiae [5], and 200 μm for pig mandible [6]). The periosteum constitutes a niche for many cells that participate in ossification during pre-natal development and fracture healing [7-9]. As the periosteum is widely recognized to be of critical importance in bone formation and regeneration, the development of a periosteum-like membrane would be a promising strategy for bone tissue engineering [10, 11]. There are only a few models of periosteum for engraftment in bone defect including natural scaffolds such as porcine small intestinal submucosa [12], decellularized periosteum [13], or vascularized biomimetic cell-sheet-engineered periosteum [14].

In the past few years, a periosteum-like environment was developed using electrospun hydroxyapatite-containing chitosan (CHI) nanofibers [15]. Polyethylene glycol (PEG) hydrogels were also used to emulate the periosteum in a murine femoral defect model [16]. Recently, free-standing (FS) microgrooved poly(lactic-co-glycolic acid) (PLGA) nanosheets were developed for the purpose of generating a biomimetic periosteum [11]. Since muscle-periosteal connection is important for periosteal healing [17], the design of a periosteum like membrane implies the elaboration of a thick membrane suitable for both muscle and bone formation.

The layer-by-layer (LbL) technique appears as a powerful tool for the engineering of FS membranes. LbL coatings offer a large range of potentialities for biomedical applications [18-21]. Their thickness and internal structure can be easily tuned depending on the molecules used as building blocks [22], the number of deposited layers, and the assembly conditions (pH, ionic strength, concentration of the polyelectrolytes). Several physico-chemical and mechanical parameters can be directly controlled including, ion permeation [23], crosslinking of the films (which changes their Young's modulus [24] but also their biodegradability properties [25], and loading of bioactive molecules [26].

Europe PMC Funders Author Manuscripts

Europe PMC Funders Author Manuscripts

To date, few studies have reported the production of polysaccharide-based FS membranes constructed via the LbL technique[27-29]. Interestingly, these FS membranes can be simply obtained using a bottom-up approach by depositing oppositely charged polysaccharides and then removing the underlying substrate [27]. When the film is deposited on a low surface energy substrate, it can further be removed in mild conditions, leading a FS membrane without the need for a post-processing step [28, 29].

Polysaccharides can interact with several growth factors via non-covalent interactions [30, 31] that can stimulate cellular proliferation, migration, and differentiation. Furthermore, trapping growth factors in a biomimetic matrix can provide a sustained release at a lower dose [32]. Indeed, CHI and alginate (ALG) based hydrogels have already been used as a delivery carrier for BMP-2 [30].

In our previous study [29], we engineered thick FS membranes (4 to 35 μm) made of CHI and ALG by tuning the deposition conditions: pH, polyelectrolyte concentration, and number of deposited layer pairs. These FS membranes were stable in a physiological buffer and enabled the partial permeation of model drugs, indicating that they may act as a reservoir for bioactive proteins. Furthermore, we showed that these membranes enabled the growth of skeletal myoblasts (C2C12), although with differences depending on the chemistry of the ending layer.

In this work, we further explored the potentiality of the FS CHI/ALG membranes as a simple model of a natural periosteum membrane. We generated CHI/AGL FS membranes with tunable mechanical properties as confirmed by dynamic mechanical analysis—modulated by chemical crosslinking. BMP-2 was then incorporated into these membranes, and its released was followed for one month. Lastly, the bioactivity of these membranes towards both myogenesis and osteogenesis was assessed *in vitro* using skeletal myoblasts and their bioactivity *in vivo* was assessed using an ectopic mouse model.

2. Materials and Methods

2.1. Materials

Chitosan, CHI, (medium molecular weight) was purchased from Sigma-Aldrich (Germany) and was purified prior to use by a reprecipitation method [33]. Briefly, CHI was purified by dissolving it in acetic acid and precipitating with NaOH (final pH ~ 8). Subsequently, the suspension was sieved, the precipitate was thoroughly washed with distilled water and rinsed twice with ethanol for about 4 h. The product was frozen at - 80 °C and lyophilized. Finally, the obtained product was milled and the CHI powder was dried at 60 °C overnight. The degree of *N*-deacetylation (DD) was found to be 78 % by the first derivative ultraviolet spectrophotometry, using both glucosamine (GluN) and *N*-acetylglucosamine (GluNAc) standards for calibration [34]. The molecular weight (M_v) was determined by viscometry in CH_3COOH 0.5 M/ $NaCH_3COO$ 0.2 M, which was found to be 770 kDa according to the Mark-Houwing theory ($k = 3.5\times10^{-4}$; $a = 0.76$) [35]. CHI was fluorescently labeled using Alexa 568 (Invitrogen) following the manufacturer's protocol, except that the reaction was carried out for 2 h at pH 6 [29]. A Sephadex G-25 size exclusion column (PD-10,

Amersham Bioscience, Sweden) was used to purify the product and remove any unbound dye.

Sodium ALG derived from brown algae (low viscosity: 136 mPa.s) was obtained from Sigma and used as received. Human recombinant BMP-2 was provided by Medtronics. BMP-2 labeled with carboxyfluorescein (BMP-2^{CF}) was used to visualize BMP-2 in FS membranes as well as to quantify its incorporation by fluorescence spectrometry [26]. All reagents and solvents were used without further purification. For staining of the cells, rhodamine phalloidin (P2141) and the anti-troponin T antibody (T6277) were purchased from Sigma. The 5-ethynyl-2′-deoxyuridine (EdU) proliferation assay (C10340) was purchased from Life technologies.

2.2. Preparation of thick (CHI/ALG) free-standing films

The different steps of the FS membrane preparation are summarized in Scheme 1. Briefly, the multilayer films were built on polypropylene substrates using freshly prepared polyelectrolyte solutions (step 1). Prior to film deposition, they were cleaned with ethanol and rinsed thoroughly with water before being dried with a stream of nitrogen. The substrate was first dipped in the CHI solution for 5 min then rinsed twice in water (both at pH 5) for 2 min. Subsequently, they were immersed in ALG solution (pH 3) for 5 min followed by rinsing twice in water (with the same pH as the ALG solution) for 2 min [29]. This procedure was repeated using a dipping robot (DR3, Kirstein and Viegler GmbH) until the deposit of 200 layer pairs was achieved. These FS membranes will be named hereafter $(CHI/ALG)_{200}$. After that, the membranes were let to dry in air and detached. For membrane crosslinking (step 2), 1-ethyl-3-(3-dimethylaminopropyl)carbodiimide hydrochloride (EDC) and N-hydroxysulfosuccinimide (s-NHS) were dissolved in milli-Q water at pH 5.5 at final concentrations of 10, 30, 50 mg/mL (for EDC) and 11 mg/mL (for s-NHS), respectively. The FS were put in contact with the freshly prepared EDC/s-NHS solution overnight at 4 °C. After that, the FS were thoroughly washed with HEPES (20 mM) at pH 7.4 and dried at RT. In the following, the FS crosslinked with EDC at 10, 30 and 50 mg/ml will be named EDC10, EDC30 and EDC50, respectively.

2.3. Fourier Transform Infrared Spectroscopy (FTIR)

The chemical structure of the dry FS membranes was studied by FTIR spectroscopy in transmission mode with a Vertex 70 spectrophotometer (BrukerOptic Gmbh, Ettlingen, Germany) equipped with a MIR detector [36]. All spectra were recorded between 400 and 4000 cm^{-1} with a 2 cm^{-1} resolution using Blackman-Harris three-term apodization and the standard Bruker OPUS/IR software v6.5 (Bruker Optic Gmbh). After detachment of the FS membrane, the spectra of the uncrosslinked and crosslinked $(CHI/ALG)_{200}$ FS films were acquired and the spectrum of air was taken as reference. The experiments were performed in duplicate with at least 4 different samples per condition in each independent experiment.

2.4. Scanning Electron Microscopy (SEM)

The morphological analysis of the uncrosslinked and crosslinked $(CHI/ALG)_{200}$ FS membranes was performed using SEM (Quanta FEG 250 FEI) where both sides of the membranes were observed in high vacuum with a Everhart-Thornley Detector (ETD

detector for secondary electrons) at an acceleration of 3 kV. For the cross section observations, the FS were dipped in liquid nitrogen until freeze fracture and the morphology was observed.

2.5. Dynamic Mechanical Analysis (DMA)

All viscoelastic measurements were performed using a Tritec2000B DMA from Triton Technology (UK), equipped with the tensile mode. The measurements were carried out at 37°C. The membrane samples were cut at ~ 4 mm in width (measured accurately for each sample). Uncrosslinked and crosslinked $(CHI/ALG)_{200}$ FS membranes were always analyzed immersed in a phosphate buffered saline (PBS) solution placed in a Teflon® reservoir. The geometry of the samples was then measured and the FS membranes were clamped in the DMA apparatus at a spacing of 10 mm and immersed in the liquid bath. After equilibration at 37°C, the DMA spectra were obtained during a frequency scan between 0.1 and 10 Hz. A static pre-load of 1 N was applied during the tests to keep the sample tight. Three specimens were tested for each condition.

2.6. BMP-2 loading and release

For the adsorption of BMP-2 on the FS membranes (scheme 1, step 3), a previously established protocol was followed [26, 37]. Briefly, the FS membranes were cut (~ 1 cm^2) and deposited into 24-well plates where they were immersed in a 1 mM HCl solution (pH = 3) for about 1 h. After removal of the HCl solution from the wells, the FS were incubated with the BMP-2 solution (overnight and at 4 °C). For the *in vitro* studies, the loading was performed with the BMP-2 solution containing 2 % of $BMP\text{-}2^{CF}$. The FS were incubated at several concentrations of BMP-2, 20 μg/mL, 60 μg/mL or 100 μg/mL and their release profiles were investigated. For EDC30 the loading was only performed at 20 μg/mL. Quantification of BMP-2 loading in and release from the FS after several washes with a HEPES buffer (20 mM, pH 7.4) was determined using a fluorescence spectrometer (Tecan Infinite 1000, Austria) as previously described [26]. Briefly, after the BMP-2 loading solution was removed from the wells, the HEPES solution was added and fluorescence of the well (including FS membrane + HEPES solution) was measured (excitation 492 nm/ emission 517 nm). At predetermined intervals, the HEPES solution in the wells was replaced by fresh HEPES solution and the fluorescence was measured. The incorporated amount was calculated based on a calibration curve obtained with known amounts of BMP-2 in solution (data not shown). The experiments were performed in duplicate, with 3 different samples for each condition in each independent experiment.

2.7. Cell culture

Murine C2C12 skeletal myoblasts (< 20 passages, obtained from the American Type Culture Collection, ATCC) were cultured in tissue culture flasks, in a 1:1 Dulbecco's Modified Eagle Medium (DMEM)/Ham's F12 medium (Gibco, Invitrogen, Cergy-Pontoise, France) supplemented with 10% fetal bovine serum (FBS, PAA Laboratories, Les Mureaux, France) containing 10 U/mL penicillin G and 10 μg/mL streptomycin (Gibco, Invitrogen, Cergy-Pontoise, France) in a 37 °C, 5% CO_2 incubator. This medium will be named hereafter

growth medium (GM). Cells were subcultured prior to reaching 60–70% confluence (approximately every 2 days).

2.8. C2C12 cell adhesion, proliferation and differentiation

Cell adhesion on the $(CHI/ALG)_{200}$ membranes was performed on 10×10 mm^2 membranes. At confluence, cells were trypsinized and seeded onto the membranes at a density of 3×10^4 cells/cm in 500 μL of medium. For this purpose, the FS membranes were maintained at the bottom of the wells using a silicone ring. The cell suspension was added on top of each immobilized membrane. In these culture conditions, the medium was able to diffuse through the membrane. To commit C2C12 toward myogenic differentiation, the cell medium was switched from GM to a differentiation medium (DM) (1:1 DMEM/F12) supplemented with 2% horse serum, containing 10 U/mL penicillin G and 10 μg/mL streptomycin.

For fluorescent staining of the cells and myotubes, C2C12 myoblasts were fixed in a solution of 3.7% of formaldehyde in Tris-NaCl buffer (TBS, 0.15 M NaCl, 50 mM Tris-HCl, pH 7.4) for 20 min and permeabilized for 4 min in TBS containing with 0.2 % of Triton X-100. Samples were blocked in TBS containing 0.1% BSA for 1 h, and were then incubated with mouse anti-troponin T (1:100) antibody in TBS containing 0.2 % gelatin for 30 min. AlexaFluor488-conjugated secondary antibody was then incubated for 30 min. The actin cytoskeleton was stained by incubation in phalloidin-rhodamine (1:800) for 30 min and nuclei were stained with DAPI (0.5 μg/ml). The fusion index of the myotubes was calculated based on troponin T as previously described [38]. Briefly, the fusion index represents the proportion of fusion events that occurs in a given condition. The higher the fusion index, the more myoconductive is the substrate. It was determined by dividing the total number of nuclei in the myotubes (minimum of 2 nuclei) by the total number of nuclei counted [38]. The results represent at least three independent experiments with 3 FS membranes per condition. More than 100 nuclei were analyzed for each condition.

The proliferation assay is based on the incorporation of the modified RNA nucleoside uridine (5-ethynyl-2′-deoxyuridine, EdU). During EdU assay, the dividing cells were stained and thus quantified to rate the proliferation of cells onto the membranes. The cells were then exposed to 10 μM EdU in culture medium for 30 min, fixed and permeabilized, and stained according to the manufacturer instructions. Experiments were performed in triplicate, with 3 different samples for each condition in each experiment.

2.9. Alkaline phosphatase (ALP) assay and mineralization assay

ALP is an early marker of osteogenic differentiation. The ALP assay determines the quantitative amount of ALP expressed by the cells, which reflects their commitment to the osteogenic pathway. BMP-2 bioactivity was assayed on C2C12 cells by quantifying their ALP expression. C2C12 cells were seeded at 90,000 cells/mL of GM onto BMP-2 loaded membranes (20 μg/mL) deposited in 24-well plates. After 3 days of culture, the culture medium was removed and the cells were washed with PBS and lysed by sonication over 5 s in 500 μL of 0.1 % Triton-X100 in PBS. 180 μL of a pH 10 buffer containing 0.1 M 2-amino-2-methyl-1-propanol (Sigma, France), 1 mM $MgCl_2$, and 9 mM p-nitrophenyl phosphate (Euromedex, France) was added to 20 μL of this lysate. The enzymatic reaction

Europe PMC Funders Author Manuscripts

was monitored in a 96-well plate by measuring the absorbance at 405 nm using a Tecan Infinite 1000 microplate reader (Tecan, Austria) over 10 min. The total protein content of each sample was determined using a bicinchoninic acid based protein assay kit (Interchim, France). The ALP activity was expressed as mmoles of p-nitrophenol produced per min per mg of protein (pnp/min/mg). The experiments were performed for cells grown on the BMP-2 loaded membranes (bBMP-2) crosslinked to different extents (EDC10, 30 and 50). A positive control was also included by adding BMP-2 in solution (soluble BMP-2, sBMP-2) for cells loaded on the unloaded FS membranes. The experiments were performed in triplicate, with 3 different samples for each condition in each independent experiment.

For mineralization, C2C12 cells were cultured on the FS membranes (loaded or not with BMP-2) for 2 weeks in GM supplemented with 50 mM ascorbic acid and 8 mM β-glycerol phosphate. Alizarin red staining was used to detect mineralization. Cells were fixed in 3.7% formaldehyde in PBS for 40 min. After rinsing with milliQ water, 500 μL of alizarin red (2% w/v in water, pH 4.2 adjusted with NaOH and HCl) was added to each sample and incubated at room temperature for 30 min then rinsed with milli-Q water. Images were taken using a microscope (Olympus bx41). Alizarin staining was quantified by converting the uncalibrated linear RGB pictures into uncalibrated linear 32-bit CMYK stack using the plugin version of Stephan Saalfeld's BeanShell script in the Image J software v1.43m (NIH). Then the magenta picture was taken as the closest to red and the integrated density was determined for each condition.

2.10. Imaging of cells and FS membranes

Cells and membranes were observed using a Zeiss LSM 700 confocal laser scanning microscope (CLSM, Carl Zeiss SAS, Le Pecq, France) in the HEPES-NaCl with a 10x or 20x air immersion objective. The membranes were deposited in between two 25 mm diameter glass coverslips in a drop of HEPES 20 mM maintained by an Attofluor chamber (Invitrogen). All image quantifications were performed using Image J software v1.43m (NIH).

2.11. Preliminary *in vivo* ectopic assay in mice

Two female NMRI nude mice (5 weeks old) weighing 24 ± 0.5 g were purchased from Janvier (Le Genest St Isle, France). Facility rooms were maintained at constant temperature and humidity (25°C, 30-50 % relative humidity) and 12 h light/dark cycle. All animal studies were conducted in accordance with European Union guidelines and approved by the regional ethics committee. 4 FS membranes crosslinked at EDC10 and EDC50 and loaded at two different BMP-2 amounts (60 and 100 μg/mL) (as described in 2.6) were used for the preliminary tests. The dry membranes were implanted subcutaneously on the back of anesthetized mice. Anesthesia was performed using 4% Isoflurane 1.5 L/m air (Axience, Pantin, France) during induction and then 2% Isoflurane for maintenance with 1 L/m air. After implantation, suture stitches were performed. Subcutaneous membrane-mediated bone formation was monitored at days 0, 9, 21, 32,42 and 52 post-implantation by whole body scanner using microCT (Viva-CT 40; Scanco Medical, Brütisselen, Switzerland) with low Resolution settings (80 μm isotropic voxel size, voltage of 70 kV and a current of 114 mA).

Quantification of bone formation was obtained using a low threshold of 150 mgHA/ccm. The region of interest was drawn around the observed new bone formations.

2.12. Statistical analysis

Data are reported as mean ± standard error of the mean and statistical comparisons were performed using SigmaPlot software. Edu, ALP and Alizarin red data were compared by *t*-test. For the fusion index, as the number of cells for each condition was not equal (much less cells in EDC 10 FS membranes), a Mann-Whitney Rank Sum Test was applied. All the conditions for the released data (different EDC and different loading concentrations) were analysed using a non-parametric Kruskal-Wallis test. Statistically different values are reported in the figures (* $p < 0.05$ was considered significant).

3. Results

3.1. Free-standing polysaccharide membranes: morphology and crosslinking

In this work, ~ 50 μm thick FS membrane made of $(CHI/ALG)_{200}$ were produced by the LbL assembly of CHI and ALG on a polypropylene substrate and subsequently detached by air drying. Such FS were easy to handle with tweezers both in dry or hydrated conditions (Figure 1A) and can be cut in the desirable shape. The $(CHI/ALG)_{200}$ FS membranes were crosslinked using EDC in order to improve their stability in liquid conditions, as LbL film stability and biodegradability can be significantly changed by chemical crosslinking [28, 39, 40]. Interestingly, this chemistry is of “zero length”, meaning that there is no additional molecule introduced in the film, the carbodiimide being simply converted to water soluble urea derivative, which has very low cytotoxicity [41, 42] and can be washed away. SEM observations of the upper side and cross-sections of the FS membranes crosslinked at different degrees (Figure 1B, B’) revealed an increased roughness when the crosslinking degree was higher. Cross-sections of the FS membranes (Figure 1B’) also revealed the homogeneous structure of the membranes.

Crosslinking of the FS membrane was characterized by FTIR and DMA. Figure 2A shows FTIR spectra of the $(CHI/ALG)_{200}$ membranes crosslinked at different degrees. Two major regions can be observed. A band at 1412 cm^{-1} corresponding to the COO^- symmetric stretch of ALG [43]. The second band between 1500 to 1700 cm^{-1} contains the COO^- asymmetric stretch of ALG at 1605 cm^{-1} [44] and the amide I band of CHI. As the EDC concentration increased, we noted a broadening of the amine I band, a decrease in the carboxylic peak at 1605 cm^{-1} as well as an increase in the C=O ester band at 1736 cm^{-1} (Figure 2A). Differences between the spectra obtained after crosslinking to the spectrum of a native membrane enabled to highlight the structural changes upon crosslinking, i.e. increase in the amide I band and decrease of COO^- peak (Figure 2A’).

DMA experiments were performed to assess the mechanical/viscoelastic behavior of the FS membranes in a physiological environment (Figure 2 B, B’). The storage (elastic) modulus *E’* and the loss factor (tan δ) were determined. *E’* was always lower than 3 MPa for the uncrosslinked membranes and crosslinked membranes at EDC10. In contrast, it was always higher than 15 MPa for all the other crosslinking conditions. *E’* increased with increasing

EDC concentration except for FS at EDC70, for which the membranes were found to be brittle. We also noted a slight increase in *E'* with increasing frequency that was also found before in pure CHI membranes [45]. The tan δ is the ratio of the amount of energy dissipated by viscous mechanisms relative to energy stored in the elastic component. It provides information about the damping properties of the membrane. The tan δ was very close for all conditions but it also exhibited a slight increase with the frequency. The native membrane and the EDC10 membranes had slightly higher dissipative properties at these higher frequencies, which can be related to their lower crosslinking degree [46].

Based on these results and on the fact that crosslinking is known to improve resistance to factors such as pH changes and enzymatic degradation [39], we selected FS membrane crosslinked at EDC10, EDC30 and EDC50 for further cellular assays.

3.2. Myogenic differentiation on crosslinked FS membranes

The C2C12 myoblasts were observed after 24 h in GM and after 5 days in DM (Figure 3A). The percentage of proliferating cells and their fusion index were quantified after 1 and 5 days, respectively (Figure 3B, C). We noted that few cells attached on EDC10 membranes, whereas they adhered, proliferated, and fused on the EDC30 and EDC50 membranes (Figure 3A). The EdU proliferation assay confirmed that the cells were metabolically active and exhibited a significant increased proliferation when the crosslinking of the FS membrane was increased (Figure 3B). After 5 days in DM on EDC10 films, cells begun to form large aggregates and there was only a few short myotubes. However, cells differentiated in long and thin myotubes on EDC30 and EDC50 crosslinked membranes (Figure 3C). The fusion index increased with the EDC concentration, from 0.23 ± 0.11 for EDC10, 0.41 ± 0.08 for EDC30 to 0.48 ± 0.03 for EDC50 FS membranes. All together, these results showed that myogenic differentiation was influenced by the crosslinking degree, the more crosslinked membranes being more myoconductive.

3.3. BMP-2 loading and release from the crosslinked FS membranes

In order to study the potentiality of the FS membranes for bone repair, we selected BMP-2 as osteoinductive growth factor [47, 48] to be loaded in the membranes. Here, we studied the potentiality of crosslinked FS membranes to trap and subsequently release BMP-2. CLSM images of the FS membranes after loading with BMP-2 are shown in Figure 4A, the FS membranes being labeled in red with Alexa568. Two layers of BMP-2 were clearly visible at the upper side (ALG ending) and bottom side of the membrane (CHI). Moreover, the BMP-2 loaded FS membranes were found to be stable and to retain their integrity when kept in HEPES at 4°C for 8 months (Figure 4A, right image).

The release kinetics of BMP-2 from the FS membranes was followed over 1 month for FS membranes loaded with BMP-2 at a concentration of 20, 60, and 100 μg/mL (Figure 4B, B', B" and Table 1). The incorporation of BMP-2 was measured initially (Γ_i) and after one month (Γ_f). For all the EDC concentrations, the incorporated amounts of BMP-2, Γ_i, significantly increased when the loading concentration of BMP-2 was higher. For instance, for EDC10 membrane, the total amount of BMP-2 loaded increased from 2.7 μg to 10.8 μg when the initial BMP-2 concentration increased from 20 μg/mL to 100 μg/mL were loaded.

Also, the initial loading of BMP-2 in the FS membranes was slightly higher for the EDC10 FS membranes than for the EDC50 FS membranes.

Regarding the release profiles, the trends were similar with a “burst” release of ~5 - 20 % (Γ_b) observed in the first 4 h, which was followed by a continuous release until reaching a plateau. To note, this burst was systematically higher for the low crosslinking (EDC10) as compared to the EDC50 ones. This was also the case for the absolute amount of BMP-2 released, which was of the order of 1 to 2 μg, and for the total % of BMP-2 released.

Point à rajouter (cf Remarque reviewer) However, the final loaded amounts Γ_f of BMP-2 remaining in the FS after extensive washes were statistically similar for EDC10 and EDC50. Globally, Γ_f increased with the initial concentration of BMP-2 in solution. A maximum of 8.8 ± 2.3 and 7.4 ± 2.3 μg/membrane for EDC 10 and EDC 50, respectively, was reached for the highest loaded BMP-2 concentration of 100 μg/mL. The EDC30 FS membranes presented an intermediate trend and were not considered for further evaluation.

All together, these results showed that the amount of BMP-2 incorporated and the corresponding release profile can be tuned depending on the initial concentration of BMP-2 in solution and on the crosslinking degree of the FS membrane.

3.4 Osteoinductive potential of FS membranes *in vitro* and *in vivo*

In vitro bioactivity of the BMP-2 loaded FS membranes were assessed using C2C12 myoblasts, these cells being an acknowledged model of osteoinduction *in vitro* [49]. We noted that cell adhesion slightly increased in presence of membrane bound BMP-2 (bBMP-2) as compared to BMP-2 added in solution (sBMP-2) (data not shown). Cell proliferation, as quantified by the EdU assay (Figure 5A), was only ~ 4 % for the EDC10 membranes and increased significantly to 17 % ± 8 % and 16% ± 6 %, respectively, for the EDC30 and EDC50 FS membranes loaded with BMP-2. Regarding the osteogenic capacity of the FS membranes, we first verified, as a negative control, that all the crosslinked FS membrane did not induce ALP activity in the absence of BMP-2 (Figure 5B **and data not shown**). The positive control consisted of soluble BMP-2 (sBMP-2) added to the cells grown on the crosslinked FS membranes. Cells were found to express a similar level of ALP on all the BMP-2 loaded FS membranes whatever the crosslinking degree, but the ALP level was lower than the positive control.

Longer term mineralization was also assessed after 1 and 2 weeks by visualizing Alizarin red staining (Figure 5C, 5C’). As anticipated, only a very low basal staining of the membranes in the absence of BMP-2 was detected for all crosslinking conditions as shown in Figure 5C’ (and data not shown). In contrast, all BMP-2 loaded membranes induced a positive staining with alizarin, indicating the presence of calcium deposits. The mineralization was visible at both time periods. However, we noted significantly higher calcium deposition on EDC10 and EDC50 in comparison to EDC30 FS membranes. Overall, these results indicated that the BMP-2 loaded FS membranes are osteoinductive *in vitro*. We selected the two extreme conditions, ie EDC10 and EDC50, which showed higher calcium deposition, for the *in vivo* preliminary study.

In order to further assess the osteoinductive potential of the BMP-2 loaded crosslinked FS membranes, a preliminary study was performed *in vivo* in a mouse ectopic model [50, 51]. We selected 4 different FS membranes crosslinked at EDC10 and EDC50 and loaded at 60 μg/mL and 100 μg/mL. Bone formation was followed *in situ* by μCT over 8 weeks (Figure 6A) and the bone volume was quantified (Figure 6B). We noted that the EDC10 FS membrane did not lead to bone formation whatever the loaded amount of BMP-2 (Figure 6 and data not shown). In contrast, a bone nodule was formed as soon as day 21 for the EDC50 FS membrane loaded with 100 μg/mL of BMP-2, which continued to grow up to day 52. These preliminary data suggest that only the EDC50 FS membrane loaded at the highest amount (100 μg/mL) exhibited osteoinductive properties *in vivo*.

4. Discussion

In this work, we developed a periosteum-like biomaterial by producing ~ 50 μm thick FS membrane made of $(CHI/ALG)_{200}$ by LbL assembly. The periosteum being a bilayer structure composed of a fibrous layer linking muscles and ligaments, and a cellular layer of osteoblastic precursors [52], a biomimetic membrane would assume the ability of being both myoconductive and osteoinductive.

The development of skeletal muscle is a multistep process, which includes initial cell adhesion, and proliferation; followed by withdrawal from the cell cycle and differentiation into multinucleated myotubes [53]. ALG has already been used as biomaterial for studying muscle cell growth [54-56]. Our previous work using the C2C12 skeletal myoblasts cultured on ALG or CHI-ending FS native membranes showed that cell adhesion was better on ALG-ending membranes [29]. Here, we found that crosslinked FS membranes were myoconductive and that myoblast proliferation and differentiation increased as a function of the crosslinking degree. Our results are consistent with previous results showing that muscle cell adhesion and proliferation, and differentiation depend on substrate stiffness [57-59]. It is here important to note that both the stiffness and roughness may influence the cell fate as we visualized by SEM that the surface of the FS membranes were rougher with increasing crosslinking degree (Figure 1B).

Delivering BMP-2 in a controlled manner is a challenge for the engineering of osteoinductive materials. It is known that the efficacy of BMP delivery systems depends on the amount of BMP delivered [60] but also on the formulation of the matrix. Commercial collagen matrices are known to poorly retain BMP-2 as 40-60% of the encapsulated protein is immediately released in the first 3 h leading to low therapeutic effect and cost-effectiveness [61-63]. In order to overcome such drawbacks, several studies have been performed to deliver BMP-2 more efficiently [64-66]. Some of these studies used bulk polymers where considerable amounts of BMP-2 are required (in the order of the milligrams). Recently, hydrogels that present a stronger affinity for BMP-2 have been developed [67, 68].

To our knowledge, very few studies aimed at delivering BMP-2 from polysaccharide-based membranes. Recently, Chung *et al* [69] produced a ~130 μm thick self-assembled membrane made of collagen with HA. The membranes were fabricated in one step by adding BMP-2 to

the collagen solution before overlaying on the top of the HA solution. They observed a slow and sustained release of BMP-2 without an initial burst release. Such behaviour was attributed to the washing steps, necessary to eliminate the excess of HA solution immediately upon membrane formation, and to both physical entrapment of BMP-2 within the collagen-HA membrane and ionic complexation between the negatively charged carboxyl groups of HA and the net positively charged BMP-2 protein. Such bonds contributed to enhance noncovalent immobilization, prolonged release of the protein, and lack of a burst release. The osteogenic potential of collagen-HA membranes at 4 weeks in a subcutaneous mouse model was shown via Von Kossa staining and immuno-staining of osteopontin and osteocalcin.

Surface coatings in the form of LbL films can be used to locally deliver BMP-2 from biomaterial surfaces [26, 51, 70]. The different strategies showed that i) the precise film architecture allowed compartmentalization of the protein, leading to a sequential release; ii) the loading of proteins can be done in mild conditions preserving their activity; iii) the release can be tuned with the number of layers.

In our previous study [29], we demonstrated that the native (CHI/ALG) FS membranes were permeable to FITC-dextran of different molecular weights. Here, we showed that BMP-2 can be loaded in crosslinked FS polysaccharide membranes. The loaded amounts can be tuned depending on the initial concentration of BMP-2 in solution and crosslinking degree of the FS membrane (figure 4 and Table 1). In view of the different parameters used by the different research groups (formulation conditions, BMP-2 doses used, loading conditions, among others), it is difficult to directly correlate our results with the other studies. The comparison with the behavior of (PLL/HA) films might be more relevant, as we followed the same protocol to load BMP-2 in the EDC crosslinked FS membranes as the one that was previously used for the crosslinked (PLL/HA) supported films [26]. In the work of Crouzier *et al*. [37], the release of BMP-2 loaded at 100 μg/mL in (PLL/HA) films deposited on macroporous β-tricalcium phosphate (TCP)/hydroxyapatite (HAP) and crosslinked (EDC10 and 50) was followed over 46 days. At the end of the study period, the amounts of BMP-2 retained were 3.2 ± 0.4 and 4.1 ± 0.7 μg/granule for films crosslinked with EDC10 and EDC50, respectively. Thus, about 75% of the initial amount loaded was released from the crosslinked film with EDC10 and 30% was released for the EDC50 condition. In a recent study, a porous titanium implant was coated using the same (PLL/HA) film [51] crosslinked with EDC (EDC10, EDC30 and EDC70) and loaded with BMP-2 at 20 and 100 μg/mL. The amount of BMP-2 incorporated could be tuned over a large range depending on both the extent of film crosslinking and on the initial BMP-2 concentration. For example, EDC10 incorporated the highest amount of BMP-2 (4.2 and 18.9 $\mu g/cm^2$ when loaded with 20 and 100 μg/ml of BMP-2, respectively). At the end of 7 days such EDC10 released 62 % and 77% of the initial incorporated amount of BMP-2 for 20 and 100 μg/ml of BMP-2, respectively. The more crosslinked films were found to load more BMP-2 and to release a lower % of it. Thus, the incorporation and release profiles we observed here are qualitatively similar, i.e. increase BMP-2 loading when the initial BMP-2 concentration is increased and increase released % for the less crosslinked film/membrane (EDC10 as compared to EDC50).

Macdonald *et al*. [71] coated a 3D scaffold by using LbL films consisting in the successive deposition of 100 tetralayers. Each tetralayer consisted of a hydrolysable poly (β-aminoester) as polycation, chondroitin sulfate as polyanion, and BMP-2 as polycation at an initial concentration of 50 μg/mL paired with chondroitin sulfate. A little burst release was observed and 80 % of BMP-2 was released over a period of 2 days and the remaining 20 % were released in a sustained way over a period of 2 weeks. In their case, the total amount of BMP-2 can be tuned depending on the number of tetralayers. Other release profiles were also discussed in literature [70, 72] using the LbL technology.

The loading of BMP-2 in our EDC50 crosslinked FS membranes led to a decrease in cell proliferation after 24 h in culture in GM (Figure 5A) as compared to the case without BMP-2 (Figure 3). This result may be explained by the differentiation commitment of the cells as they exit the cell cycle to commit to osteogenesis. Indeed, this finding is corroborated with the ALP activity after 3 days in culture. Our results, regarding the decrease of proliferation, are consistent with the results obtained by Cheung et al [69] for the collagen/HA membranes loaded with BMP-2.

The results of the preliminary *in vivo* study in an ectopic site of nude mice revealed differences between the FS membranes according to their crosslinking degree and incorporated BMP-2 amount. To note, we have already shown that, in the absence of BMP-2, a polysaccharide film cannot be in itself osteoinductive [51]. Here, the EDC10 membranes did not lead to a visible bone nodule formation even after 52 days. In contrast, EDC50 membranes led to observable bone formation as early as 21 days of implantation in the vicinity of the membrane (Figure 6A), but only for the highest BMP-2 loaded concentration. In view of the different loading and release profiles of the FS membranes (Table 1 and Figure 4), several hypothesis may be made: first, these differences in osteoinduction may be due to the different release kinetics *in vivo*; second, they may be due to a different bioactivity of the BMP-2 released from the cross-linked membranes; third, the biodegradability of the FS polysaccharide membranes *in vivo* may play a role, as *in vivo* biodegradability of CHI/HA films was previously shown to depend on the crosslinking degree [25].

Several studies have shown that a carrier incorporating BMP-2 can induce bone formation in an ectopic site by activating a set of cellular events [50, 69, 71, 73, 74]. Although all these studies observed bone formation, the amount of BMP-2 incorporated in the carriers and the time in which osteogenesis occurred were always different. Usually, *in vivo* experiments using rat (subcutaneous back) and rabbit (intramuscular) as animal models revealed bone formation usually after 4 weeks. Kisiel *et al* [74] in a rat ectopic model using an injectable hyaluronic acid hydrogel as BMP carrier (20 μg/mL) observed bone formation after 7 weeks. Here we found bone formation at 3 weeks. In all cases, it seems that the induction of bone formation requires a local retention of BMP-2, a release over a prolonged period and exposure to the surrounding cells. In future studies, we aim to follow the biodegradability of the FS membrane as well as BMP-2 release *in vivo*. In addition, the next step will be to study their osteoinductive properties in a bone site.

Conclusions

In summary, FS membranes made of polysaccharides CHI and ALG were crosslinked chemically using EDC, which improved their mechanical properties. The crosslinked membranes enabled the proliferation of skeletal myoblasts and their subsequent differentiation in myotubes, a process that depended on the crosslinking extent. Furthermore, the crosslinked FS membranes could be loaded with the osteoinductive growth factor BMP-2. The amount of BMP-2 loaded as well as the release profile was tuned depending on the EDC concentration and on the initial concentration of BMP-2 in solution. After an initial burst, the growth factor was released over a month by diffusion. The osteoinductive capacity of the FS membranes was proved *in vitro* by the ALP test and mineralization assays. Besides, preliminary *in vivo* data suggest that the EDC50 FS membrane was osteo-inductive in a mouse ectopic model after 21 days. We believe that these myoconductive and osteoinductive membranes will open new perspectives for future *in vivo* studies as tissue engineered constructs for the repair of bone fractures.

Acknowledgements

This work was financially supported by Foundation for Science and Technology (FCT) through the scholarship SFRH/BPD/96797/2013 granted to Sofia G. Caridade. CM is indebted to Association Française contre les Myopathies for financial support via a post-doctoral fellowship (AFM project 16673). JA acknowledges the Whitaker International Fellows and Scholars Program for support via a post-doctoral fellowship. This work was supported by the European Commission (FP7 program) via a European Research Council starting grant (BIOMIM, GA 259370 to CP) and by the AFM (grant Microtiss, 16530). We thank Isabelle Paintrand for her technical help with the confocal apparatus.

References

[1]. Ma PX. Biomimetic materials for tissue engineering. Adv Drug Deliv Rev. 2008; 60:184–98. [PubMed: 18045729]

[2]. Nikkhah M, Edalat F, Manoucheri S, Khademhosseini A. Engineering microscale topographies to control the cell-substrate interface. Biomaterials. 2012; 33:5230–46. [PubMed: 22521491]

[3]. Paulsson M. Basement Membrane Proteins: Structure, Assembly, and Cellular Interactions. Crit Rev Biochem Mol. 1992; 27:93–127.

[4]. Sakai D, Kii I, Nakagawa K, Matsumoto HN, Takahashi M, Yoshida S, et al. Remodeling of Actin Cytoskeleton in Mouse Periosteal Cells under Mechanical Loading Induces Periosteal Cell Proliferation during Bone Formation. PLoS One. 2011; 6

[5]. Moore SR, Milz S, Tate MLK. Periosteal thickness and cellularity in mid-diaphyseal cross-sections from human femora and tibiae of aged donors. J Anat. 2014; 224:142–9. [PubMed: 24175932]

[6]. Al-Qtaitat A, Shore RC, Aaron JE. Structural changes in the ageing periosteum using collagen III immuno-staining and chromium labelling as indicators. J Musculoskel Neuron. 2010; 10:112–23.

[7]. Arnsdorf EJ, Jones LM, Carter DR, Jacobs CR. The Periosteum as a Cellular Source for Functional Tissue Engineering. Tissue Eng Part A. 2009; 15:2637–42. [PubMed: 19207046]

[8]. Chang H, Tate MLK. Concise Review: The Periosteum: Tapping into a Reservoir of Clinically Useful Progenitor Cells. Stem Cell Transl Med. 2012; 1:480–91.

[9]. Ueno T, Kagawa T, Mizukawa N, Nakamura H, Sugahara T, Yamamoto T. Cellular origin of endochondral ossification from grafted periosteum. The Anatomical Record. 2001; 264:348–57. [PubMed: 11745090]

[10]. Cuthbert RJ, Churchman SM, Tan HB, McGonagle D, Jones E, Giannoudis PV. Induced periosteum a complex cellular scaffold for the treatment of large bone defects. Bone. 2013; 57:484–92. [PubMed: 23954755]

[11]. Shi X, Fujie T, Saito A, Takeoka S, Hou Y, Shu Y, et al. Periosteum-Mimetic Structures Made from Freestanding Microgrooved Nanosheets. Adv Mat. 2014; 26:3290–6.

[12]. Zhao L, Zhao J, Wang S, Xia Y, Liu J, He J, et al. Evaluation of immunocompatibility of tissue-engineered periosteum. Biomed Mater. 2011; 6

[13]. Rapp SJ, Jones DC, Gerety P, Taylor JA. Repairing critical-sized rat calvarial defects with progenitor cell-seeded acellular periosteum: A novel biomimetic scaffold. Surgery. 2012; 152:595–605. [PubMed: 22959744]

[14]. Kang Y, Ren L, Yang Y. Engineering Vascularized Bone Grafts by Integrating a Biomimetic Periosteum and Î2-TCP Scaffold. ACS Appl Mater Interfaces. 2014; 6:9622–33. [PubMed: 24858072]

[15]. Frohbergh ME, Katsman A, Botta GR, Lazarovici P, Schauer CL, Wegst UGK, et al. Electrospun hydroxyapatite-containing chitosan nanofibers crosslinked with genipin for bone tissue engineering. Biomaterials. 2012; 33:9167–78. [PubMed: 23022346]

[16]. Hoffman MD, Benoit DSW. Emerging Ideas: Engineering the Periosteum: Revitalizing Allografts by Mimicking Autograft Healing. Clin Orthop Relat R. 2013; 471:721–6.

[17]. Utvag SE, Grundnes O, Reikeras O. Effects of lesion between bone, periosteum and muscle on fracture healing in rats. Acta Orthop. 1998; 69:177–80.

[18]. Decher G, Hong JD, Schmitt J. Buildup of ultrathin multilayer films by a self-assembly process: III. Consecutively alternating adsorption of anionic and cationic polyelectrolytes on charged surfaces. Thin Solid Films. 1992; 210/211(Part 2):831–5.

[19]. Tang ZY, Wang Y, Podsiadlo P, Kotov NA. Biomedical applications of layer-by-layer assembly: From biomimetics to tissue engineering. Adv Mat. 2006; 18:3203–24.

[20]. Boudou T, Crouzier T, Ren K, Blin G, Picart C. Multiple functionalities of polyelectrolyte multilayer films: new biomedical applications. Adv Mat. 2010; 22:441–67.

[21]. Costa RR, Mano JF. Polyelectrolyte multilayered assemblies in biomedical technologies. Chem Soc Rev. 2014; 43:3453–79. [PubMed: 24549278]

[22]. Crouzier T, Boudou T, Picart C. Polysaccharide-based polyelectrolyte multilayers. Curr Opin Colloid Interface Sci. 2010; 15:417–26.

[23]. Lutkenhaus JL, Hrabak KD, McEnnis K, Hammond PT. Elastomeric flexible free-standing hydrogen-bonded nanoscale assemblies. J Am Chem Soc. 2005; 127:17228–34. [PubMed: 16332070]

[24]. Schneider A, Francius G, Obeid R, Schwinté P, Hemmerlé J, Frisch B, et al. Polyelectrolyte Multilayers with a Tunable Young's Modulus: Influence of Film Stiffness on Cell Adhesion. Langmuir. 2006; 22:1193–200. [PubMed: 16430283]

[25]. Picart C, Schneider A, Etienne O, Mutterer J, Schaaf P, Egles C, et al. Controlled degradability of polysaccharide multilayer films in vitro and in vivo. Adv Funct Mater. 2005; 15:1771–80.

[26]. Crouzier T, Ren K, Nicolas C, Roy C, Picart C. Layer-By-Layer Films as a Biomimetic Reservoir for rhBMP-2 Delivery: Controlled Differentiation of Myoblasts to Osteoblasts. Small. 2009; 5:598–608. [PubMed: 19219837]

[27]. Lavalle P, Boulmedais F, Ball V, Mutterer J, Schaaf P, Voegel JC. Free standing membranes made of biocompatible polyelectrolytes using the layer by layer method. J Membr Sci. 2005; 253:49–56.

[28]. Larkin AL, Davis RM, Rajagopalan P. Biocompatible, Detachable, and Free-Standing Polyelectrolyte Multilayer Films. Biomacromolecules. 2010; 11:2788–96. [PubMed: 20815399]

[29]. Caridade SG, Monge C, Gilde F, Boudou T, Mano JF, Picart C. Free-Standing Polyelectrolyte Membranes Made of Chitosan and Alginate. Biomacromolecules. 2013; 14:1653–60. [PubMed: 23590116]

[30]. Lee K, Silva EA, Mooney DJ. Growth factor delivery-based tissue engineering: general approaches and a review of recent developments. J R Soc Interface. 2011; 8:153–70. [PubMed: 20719768]

[31]. Hudalla GA, Murphy WL. Biomaterials that Regulate Growth Factor Activity via Bioinspired Interactions. Adv Funct Mater. 2011; 21:1754–68. [PubMed: 21921999]

[32]. Li RH, Wozney JM. Delivering on the promise of bone morphogenetic proteins. Trends Biotech. 2001; 19:255–65.

[33]. da Silva RMP, Mano JF, RL R. Straightforward determination of the degree of N-acetylation of chitosan by means of first-derivative UV spectrophotometry. Macromol Chem Phys. 2008; 209

[34]. da Silva RMP, Mano JF, Reis RL. Straightforward determination of the degree of N-acetylation of chitosan by means of first-derivative UV spectrophotometry. Macromolecular Chemistry & Physics. 2008; 209:1463–72.

[35]. Terbojevich M, Cosani A, Muzzarelli RAA. Molecular parameters of chitosans depolymerized with the aid of papain. Carbohydr Polym. 1996; 29:63–8.

[36]. Crouzier T, Picart C. Ion Pairing and Hydration in Polyelectrolyte Multilayer Films Containing Polysaccharides. Biomacromolecules. 2009; 10:433–42. [PubMed: 19199579]

[37]. Crouzier T, Sailhan Fdr, Becquart P, Guillot R, Logeart-Avramoglou D, Picart C. The performance of BMP-2 loaded TCP/HAP porous ceramics with a polyelectrolyte multilayer film coating. Biomaterials. 2011; 32:7543–54. [PubMed: 21783243]

[38]. Charrasse S, Comunale F, Fortier M, Portales-Casamar E, Debant A, Gauthier-Rouviere C. M-cadherin activates Rac1 GTPase through the Rho-GEF trio during myoblast fusion. Mol Biol Cell. 2007; 18:1734–43. [PubMed: 17332503]

[39]. Richert L, Boulmedais F, Lavalle P, Mutterer J, Ferreux E, Decher G, et al. Improvement of Stability and Cell Adhesion Properties of Polyelectrolyte Multilayer Films by Chemical Cross-Linking. Biomacromolecules. 2004; 5:284–94. [PubMed: 15002986]

[40]. Picart C, Elkaim R, Richert L, Audoin F, Arntz Y, Da Silva Cardoso M, et al. Primary Cell Adhesion on RGD-Functionalized and Covalently Crosslinked Thin Polyelectrolyte Multilayer Films. Adv Funct Mater. 2005; 15:83–94.

[41]. Tomihata K, Ikada Y. Crosslinking of hyaluronic acid with water-soluble carbodiimide. J Biomed Mater Res. 1997; 37:243–51. [PubMed: 9358318]

[42]. Taguchi T, Ikoma T, Tanaka J. An improved method to prepare hyaluronic acid and type II collagen composite matrices. J Biomed Mater Res. 2002; 61:330–6. [PubMed: 12007214]

[43]. Valentin R, Bonelli B, Garrone E, Di Renzo F, Quignard F. Accessibility of the functional groups of chitosan aerogel probed by FT-IR-monitored deuteration. Biomacromolecules. 2007; 8:3646–50. [PubMed: 17910493]

[44]. Lawrie G, Keen I, Drew B, Chandler-Temple A, Rintoul L, Fredericks P, et al. Interactions between alginate and chitosan biopolymers characterized using FTIR and XPS. Biomacromolecules. 2007; 8:2533–41. [PubMed: 17591747]

[45]. Mano JF. Viscoelastic properties of chitosan with different hydration degrees as studied by dynamic mechanical analysis. Macromol Biosci. 2008; 8:69–76. [PubMed: 17902189]

[46]. Alves NM, Ribelles JLG, Tejedor JAG, Mano JF. Viscoelastic behavior of poly(methyl methacrylate) networks with different cross-linking degrees. Macromolecules. 2004; 37:3735–44.

[47]. Urist MR. Bone: Formation by Autoinduction. Science. 1965; 150:893–9. [PubMed: 5319761]

[48]. Wozney JM, Rosen V, Celeste AJ, Mitsock LM, Whitters MJ, Kriz RW, et al. Novel regulators of bone-formation - molecular clones and activities. Science. 1988; 242:1528–34. [PubMed: 3201241]

[49]. Katagiri T, Yamaguchi A, Komaki M, Abe E, Takahashi N, Ikeda T, et al. Bone morphogenetic protein-2 converts the differentiation pathway of C2C12 myoblasts into the osteoblast lineage. J Cell Biol. 1994; 127:1755–66. [PubMed: 7798324]

[50]. Hsu HP, Zanella JM, Peckham SM, Spector M. Comparing ectopic bone growth induced by rhBMP-2 on an absorbable collagen sponge in rat and rabbit models. Journal of Orthopaedic Research. 2006; 24:1660–9. [PubMed: 16779816]

[51]. Guillot R, Gilde F, Becquart P, Sailhan F, Lapeyrere A, Logeart-Avramoglou D, et al. The stability of BMP loaded polyelectrolyte multilayer coatings on titanium. Biomaterials. 2013; 34:5737–46. [PubMed: 23642539]

[52]. Augustin G, Antabak A, Davila S. The periosteum Part 1: Anatomy, histology and molecular biology (Retracted Article. See vol 39, pg 824, 2008). Injury-International Journal of the Care of the Injured. 2007; 38:1115–30.

[53]. Andrés V, Walsh K. Myogenin expression, cell cycle withdrawal, and phenotypic differentiation are temporally separable events that precede cell fusion upon myogenesis. The Journal of Cell Biology. 1996; 132:657–66. [PubMed: 8647896]

[54]. Rowley JA, Mooney DJ. Alginate type and RGD density control myoblast phenotype. J Biomed Mater Res. 2002; 60:217–23. [PubMed: 11857427]

[55]. Boontheekul T, Hill EE, Kong HJ, Mooney DJ. Regulating myoblast phenotype through controlled gel stiffness and degradation. Tissue Eng. 2007; 13:1431–42. [PubMed: 17561804]

[56]. Rossi CA, Pozzobon M, De Coppi P. Advances in musculoskeletal tissue engineering Moving towards therapy. Organogenesis. 2010; 6:167–72. [PubMed: 21197219]

[57]. Engler AJ, Griffin MA, Sen S, BÃ¶nnemann CG, Sweeney HL, Discher DE. Myotubes differentiate optimally on substrates with tissue-like stiffness: pathological implications for soft or stiff microenvironments. The Journal of Cell Biology. 2004; 166:877–87. [PubMed: 15364962]

[58]. Gilbert PM, Havenstrite KL, Magnusson KEG, Sacco A, Leonardi NA, Kraft P, et al. Substrate Elasticity Regulates Skeletal Muscle Stem Cell Self-Renewal in Culture. Science. 2010; 329:1078–81. [PubMed: 20647425]

[59]. Ren K, Crouzier T, Roy C, Picart C. Polyelectrolyte Multilayer Films of Controlled Stiffness Modulate Myoblast Cell Differentiation. Adv Funct Mater. 2008; 18:1378–89. [PubMed: 18841249]

[60]. Wozney JM, Rosen V, Byrne M, Celeste AJ, Moutsatsos I, Wang EA. Growth factors influencing bone development. J Cell Sci. 1990; 1990:149–56.

[61]. Uludag H, Gao T, Porter TJ, Friess W, Wozney JM. Delivery Systems for BMPs: Factors Contributing to Protein Retention at an Application Site. The Journal of Bone & Joint Surgery. 2001; 83:S128–S35. [PubMed: 11314790]

[62]. Zara JN, Siu RK, Zhang XL, Shen J, Ngo R, Lee M, et al. High Doses of Bone Morphogenetic Protein 2 Induce Structurally Abnormal Bone and Inflammation In Vivo. Tissue Eng Part A. 2011; 17:1389–99. [PubMed: 21247344]

[63]. Carragee EJ, Hurwitz EL, Weiner BK. A critical review of recombinant human bone morphogenetic protein-2 trials in spinal surgery: emerging safety concerns and lessons learned. Spine J. 2011; 11:471–91. [PubMed: 21729796]

[64]. Geiger M, Li RH, Friess W. Collagen sponges for bone regeneration with rhBMP-2. Adv Drug Deliv Rev. 2003; 55:1613–29. [PubMed: 14623404]

[65]. Li C, Vepari C, Jin H-J, Kim HJ, Kaplan DL. Electrospun silk-BMP-2 scaffolds for bone tissue engineering. Biomaterials. 2006; 27:3115–24. [PubMed: 16458961]

[66]. Kempen DHR, Lu L, Hefferan TE, Creemers LB, Maran A, Classic KL, et al. Retention of in vitro and in vivo BMP-2 bioactivities in sustained delivery vehicles for bone tissue engineering. Biomaterials. 2008; 29:3245–52. [PubMed: 18472153]

[67]. Kisiel M, Martino MM, Ventura M, Hubbell JA, Hilborn J, Ossipov DA. Improving the osteogenic potential of BMP-2 with hyaluronic acid hydrogel modified with integrin-specific fibronectin fragment. Biomaterials. 2013; 34:704–12. [PubMed: 23103154]

[68]. Martinez-Sanz E, Ossipov DA, Hilborn J, Larsson S, Jonsson KB, Varghese OP. Bone reservoir: Injectable hyaluronic acid hydrogel for minimal invasive bone augmentation. J Control Release. 2011; 152:232–40. [PubMed: 21315118]

[69]. Chung EJ, Chien KB, Aguado BA, Shah RN. Osteogenic Potential of BMP-2-Releasing Self-Assembled Membranes. Tissue Eng Part A. 2013; 19:2664–73. [PubMed: 23790163]

[70]. Shah NJ, Macdonald ML, Beben YM, Padera RF, Samuel RE, Hammond PT. Tunable dual growth factor delivery from polyelectrolyte multilayer films. Biomaterials. 2011; 32:6183–93. [PubMed: 21645919]

[71]. Macdonald ML, Samuel RE, Shah NJ, Padera RF, Beben YM, Hammond PT. Tissue integration of growth factor-eluting layer-by-layer polyelectrolyte multilayer coated implants. Biomaterials. 2011; 32:1446–53. [PubMed: 21084117]

[72]. Shah NJ, Hong J, Hyder MN, Hammond PT. Osteophilic Multilayer Coatings for Accelerated Bone Tissue Growth. Adv Mat. 2012; 24:1445–50.

[73]. Yamamoto M, Takahashi Y, Tabata Y. Controlled release by biodegradable hydrogels enhances the ectopic bone formation of bone morphogenetic protein. Biomaterials. 2003; 24:4375–83. [PubMed: 12922150]

[74]. Kisiel M, Ventura M, Oommen OP, George A, Walboomers XF, Hilborn Jn, et al. Critical assessment of rhBMP-2 mediated bone induction: An in vitro and in vivo evaluation. J Control Release. 2012; 162:646–53. [PubMed: 22902595]

Europe PMC Funders Author Manuscripts

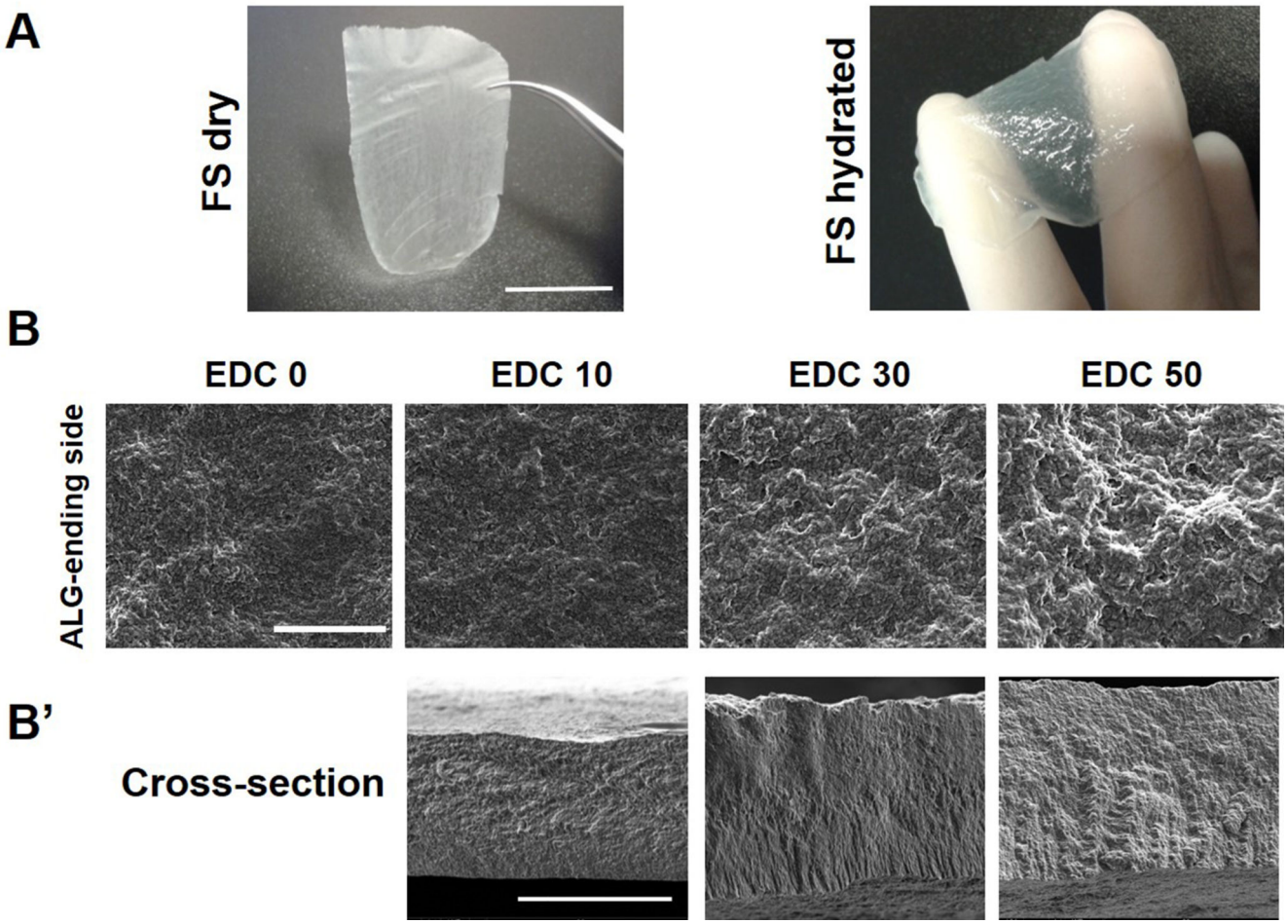

FIGURE 1. Optical microscopy and SEM images of free-standing $(CHI/ALG)_{200}$ membranes

(A) Images of a dry (left) or hydrated (right) $(CHI/ALG)_{200}$ free-standing membrane. Scale bar: 1 cm. (B) SEM observations of the upper side of the native $(CHI/ALG)_{200}$ membrane and for the FS membranes crosslinked at increasing concentration of EDC from 10 to 50 mg/mL. Scale bar is 10 μm. (B') Corresponding cross-sections of the crosslinked FS membranes. Scale bar: 20 μm.

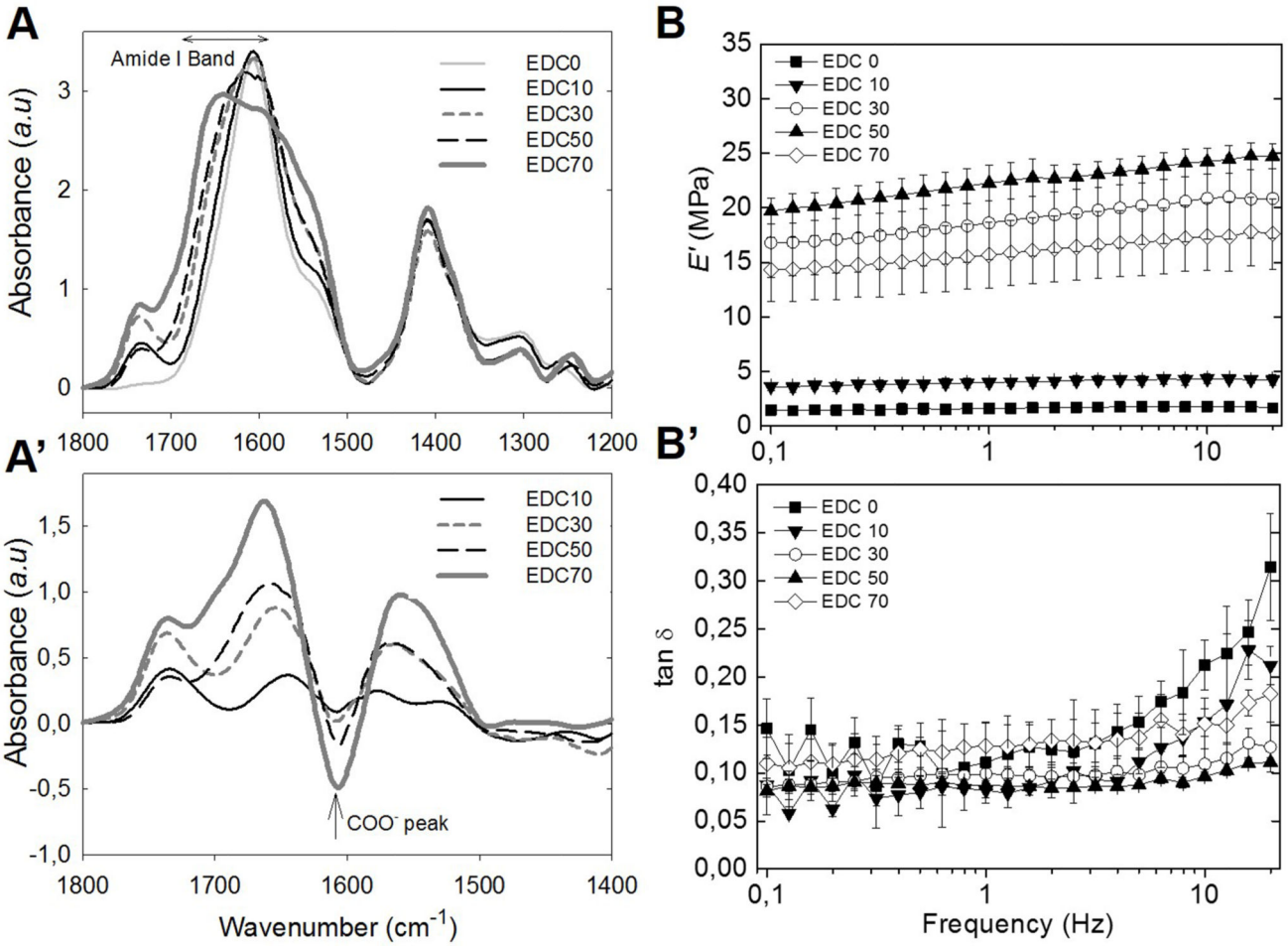

FIGURE 2. Crosslinking and mechanical properties of the FS membranes

(A) FTIR spectra of native and crosslinked $(CHI/ALG)_{200}$ FS membranes obtained at increasing EDC concentrations and (A') differences between the spectra of the crosslinked FS membranes to that of the native membrane. (B, B') Results of the DMA experiments performed at 37°C in PBS over 0.1 to 20 Hz. (B) Variation of the storage modulus (*E*') and (B') of the loss factor (tan δ).

Europe PMC Funders Author Manuscripts

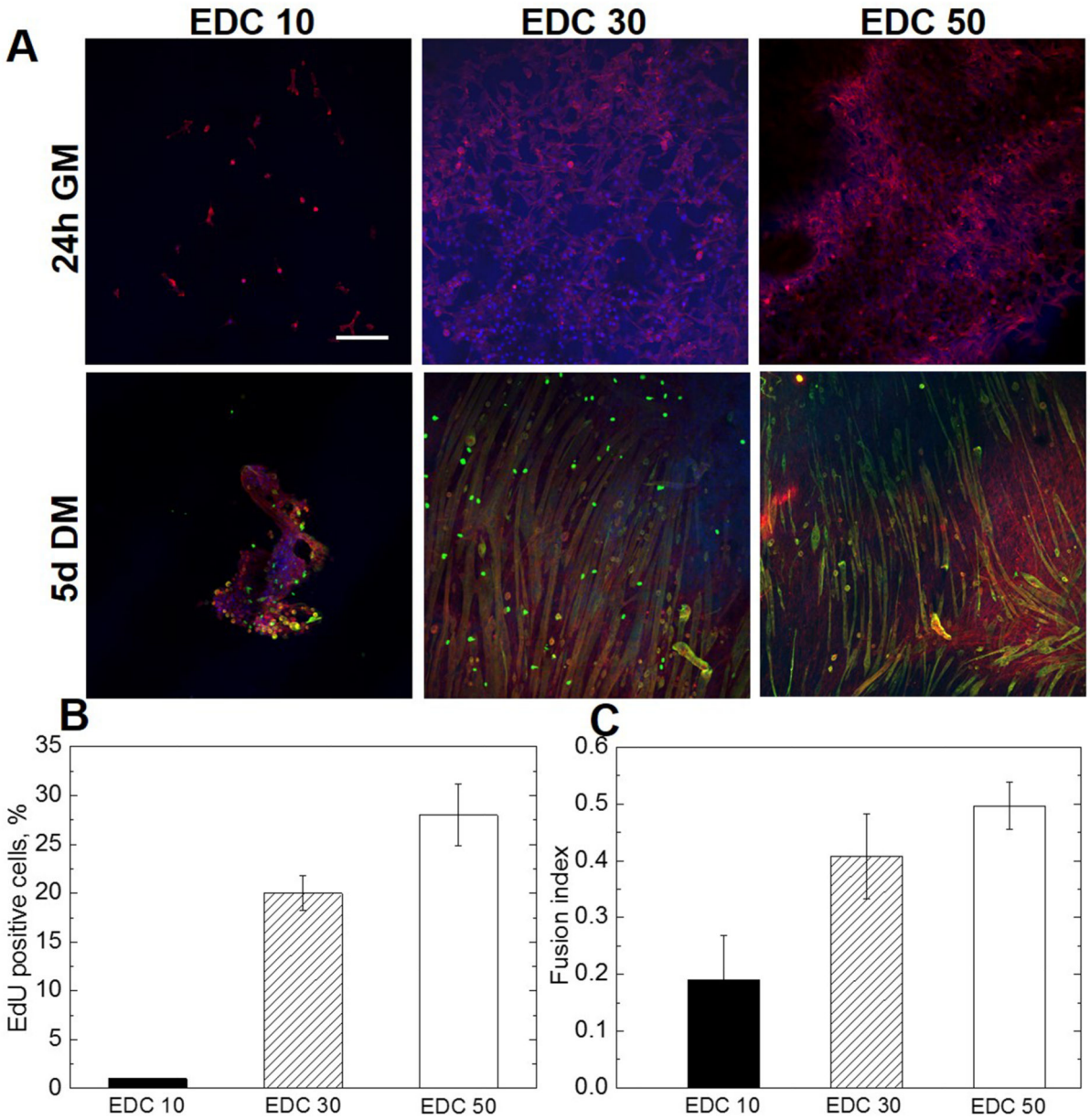

FIGURE 3. C2C12 myoblast proliferation and differentiation on the FS polysaccharide membranes

Cells were cultured on the FS membranes crosslinked at EDC10, EDC30 and EDC50. (A) CLSM images of C2C12 myoblasts were taken after 24 h in GM and after 5 days in DM. The actin cytoskeleton was stained with rhodamine-phalloidin, the nuclei were stained with DAPI and the myotubes with troponin T. Scale bar is 200 μm. (B) % of proliferating cells measured by the EdU assay after 24 h in GM and (C) Quantification of the fusion index after 5 days in DM on EDC10, EDC30 and EDC50 FS membranes (mean ± SEM of three independent experiments, * $p < 0.05$).

Europe PMC Funders Author Manuscripts

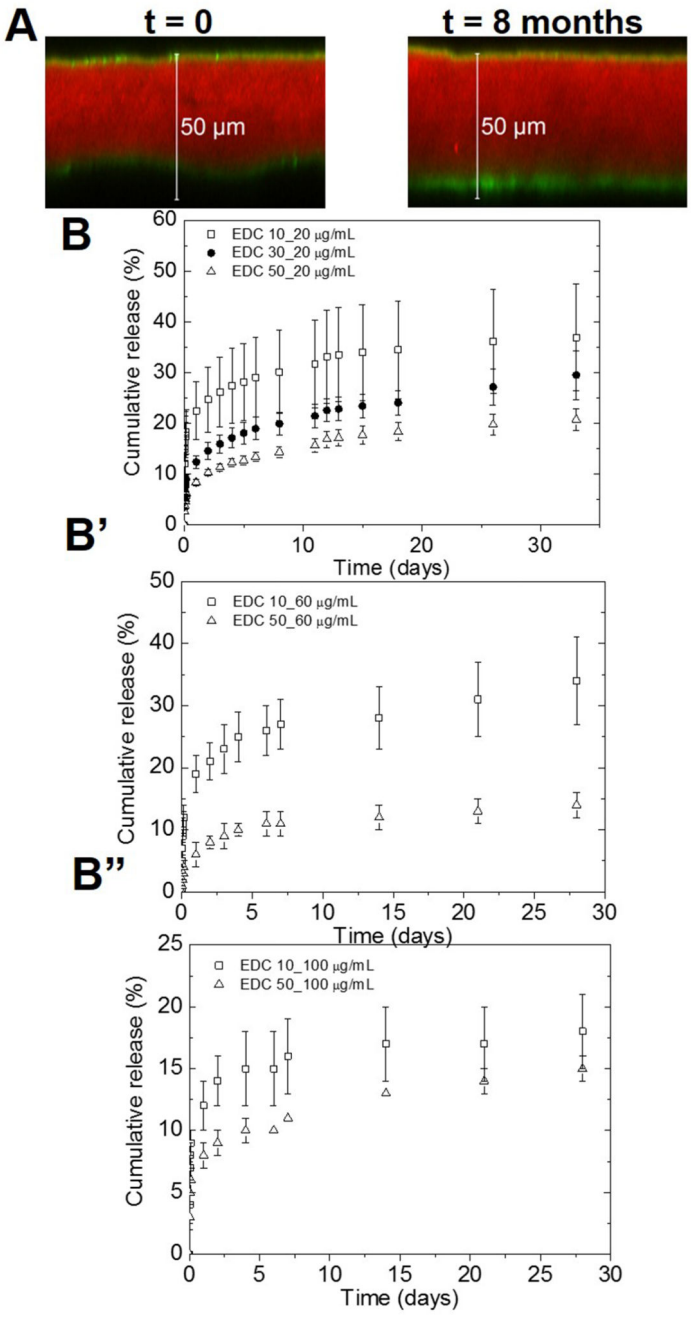

FIGURE 4.

Quantification of BMP-2 loaded in and released from the (CHI/ALG) FS membranes. (A) CLSM images of the EDC50 FS membrane labeled with Alexa 568 (red) and loaded with BMP-2 ^{CF} (green). Two BMP-2 layers on the lower and upper side of the membrane were observed over a period of 8 months. (B) Release profiles of the EDC10, EDC30, and EDC50 FS membranes over a period of one month for an initial BMP-2 loading concentration of 20 µg/ml; (B', B") Release profiles of the EDC10 and EDC50 FS membranes over a period of

one month for an initial BMP-2 loading concentration of 60 μg/ml (B') and 100 μg/ml (B"). (mean ± SEM of three samples).

Europe PMC Funders Author Manuscripts

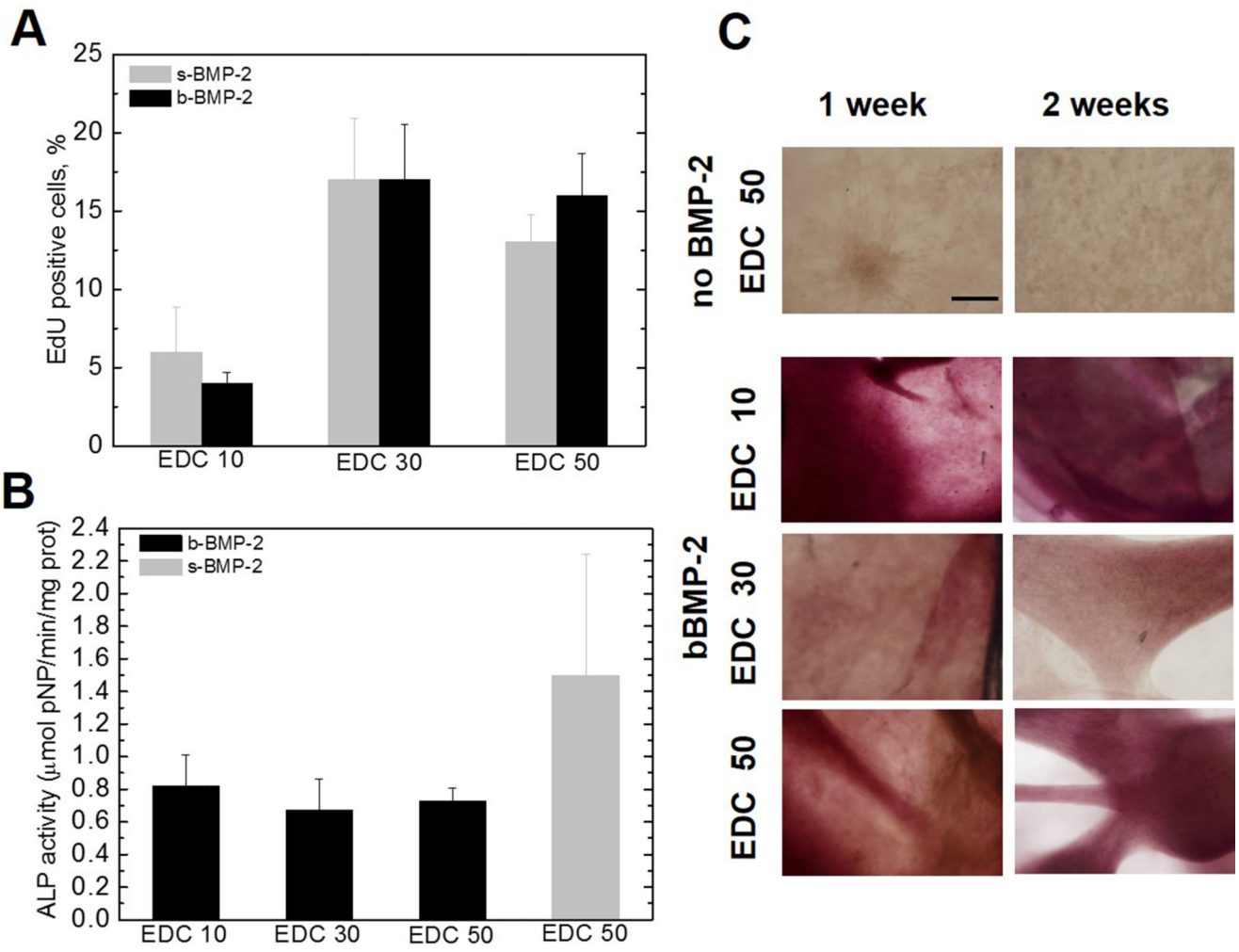

FIGURE 5.

Proliferation and osteogenic differentiation of C2C12 myoblasts on BMP-2 loaded FS membranes. (A) Quantification of myoblast proliferation after 24 h of culture in GM in absence or in the presence of BMP-2 loaded in the FS membranes (samples in triplicate, *n* = 3) or added in solution to the cells. (B) ALP activity of C2C12 myoblasts cultured for 3 days on the BMP-2 loaded membranes crosslinked at EDC10, 30 and 50 (BMP-2 was loaded at 20 µg/ml on the FS membranes) in comparison to a FS membrane in the presence of soluble BMP-2 (positive control, BMP-2 added at 600 ng/mL) (triplicate, *n*=3). (C) Microscopic images of alizarin red staining showing C2C12 cell mineralization in contact with the crosslinked FS membranes after 1 and 2 weeks in culture. Upper panel: myoblasts on FS membranes in the absence of BMP-2, showing no mineralization. Lower panels: cell mineralization on BMP-2 loaded FS membranes, the membranes crosslinked at EDC10, EDC30 or EDC50. (*n* = 3). Scale bar is 200 µm. (C') Quantification of alizarin red from groups of pictures shown in (C). (* $p < 0.05$).

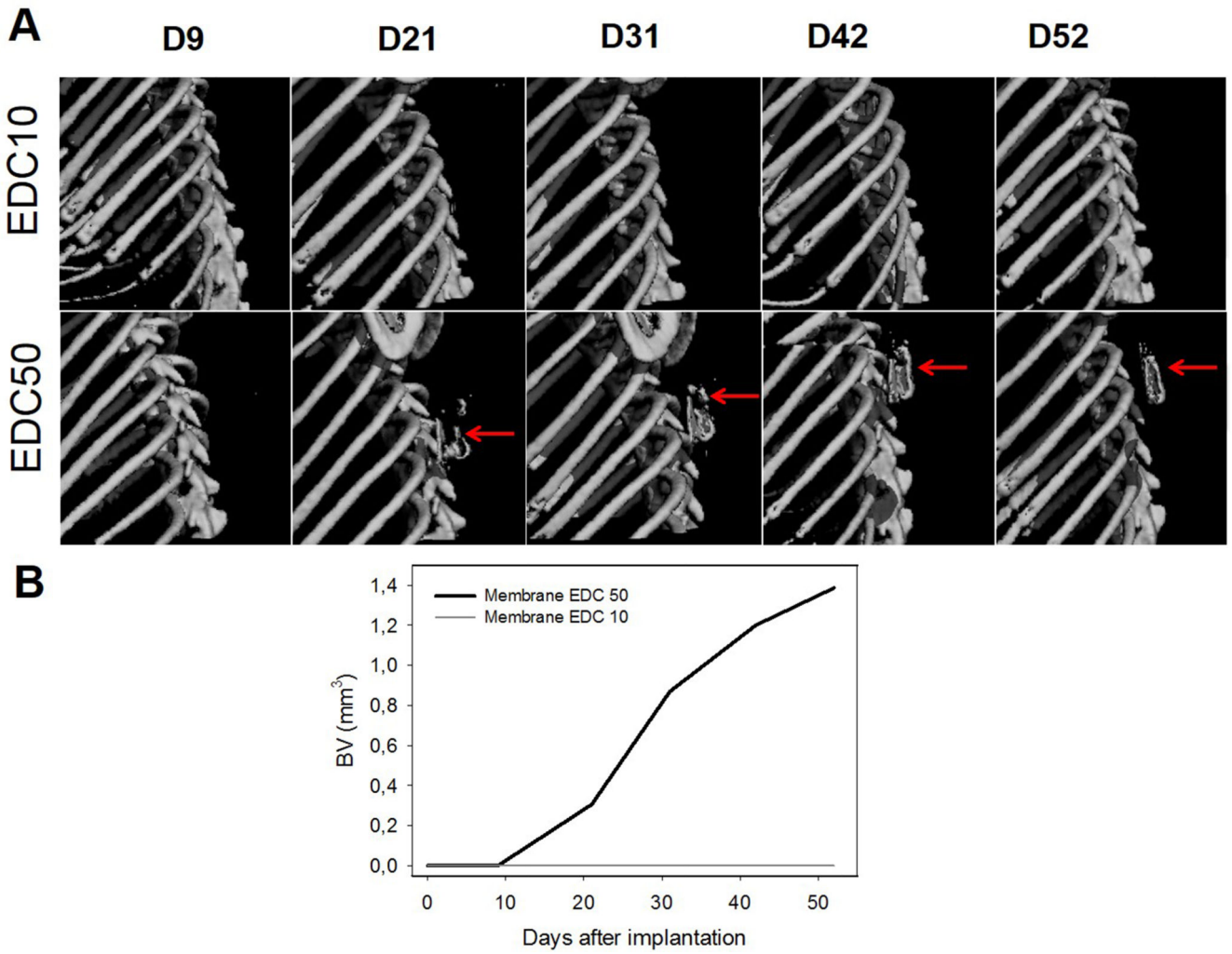

FIGURE 6.

(A) Time lapse MicroCT imaging of bone formation for BMP-2 loaded crosslinked FS membranes implanted under the skin of mice, followed at regular time intervals up to day 52. The bone nodule forming in the case of the EDC50 FS membrane is indicated with a red arrow. (B) Quantification of the bone volume as a function of time for the EDC10 and EDC50 BMP-2 loaded FS membranes. No bone formation was detected for the EDC10 FS membrane.

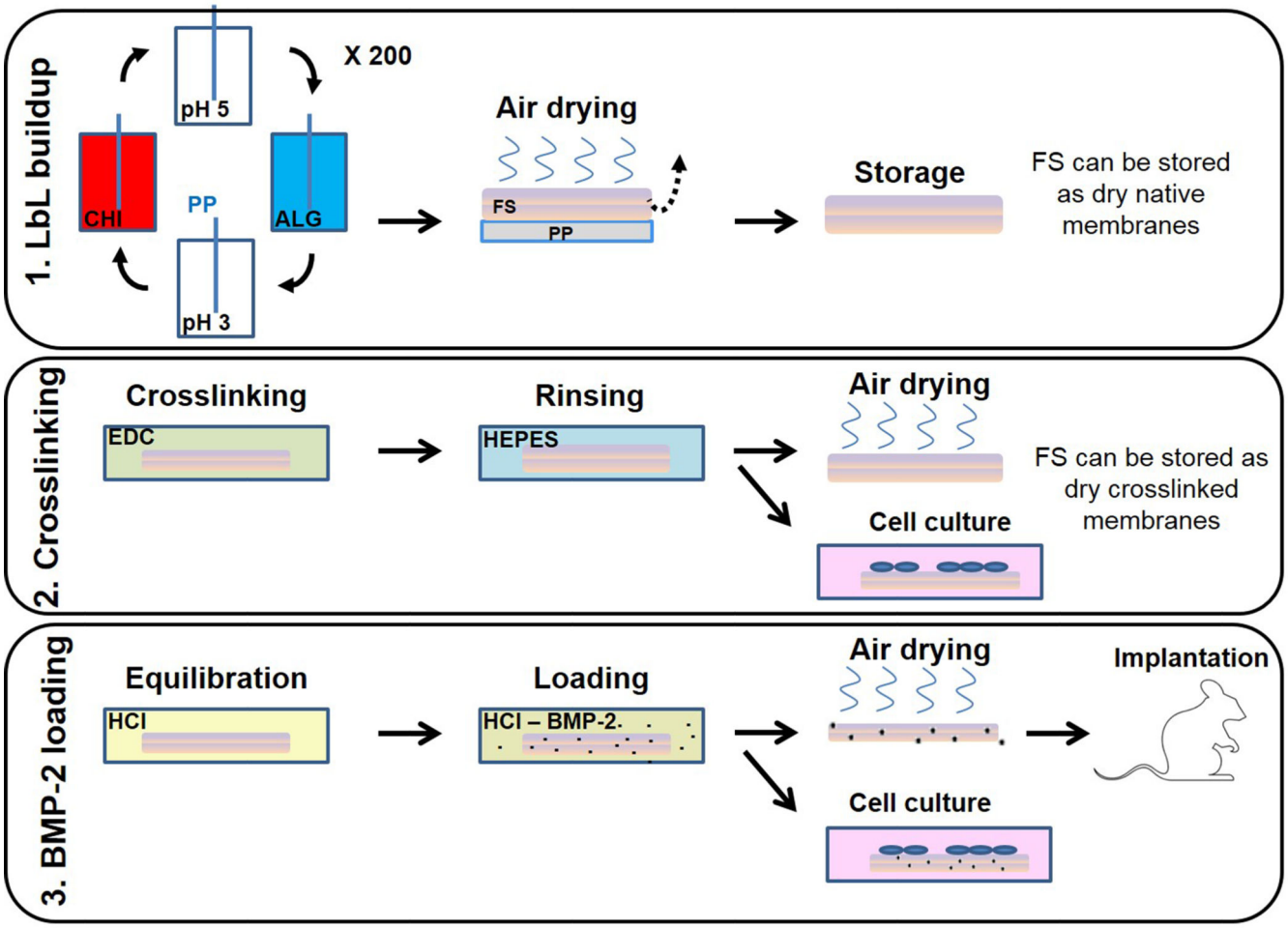

SCHEME 1.

Different steps of the preparation of the $(CHI/ALG)_{200}$ free-standing (FS) membranes. 1. The film is built on a polypropylene (PP) substrate before being air dried, detached and stored. 2. The FS membrane is crosslinked using EDC and rinsed; it is then used for the myoblast culture. 3. The FS membrane is subsequently loaded with BMP-2; its osteoinductive properties are assessed *in vitro* and *in vivo* in mice. After step 2 and 3 of the procedure, the FS membrane can be stored in dry state.

Europe PMC Funders Author Manuscripts

Table 1

Loading and released amounts of BMP-2 in and out of the FS membrane, as a function of the crosslinking degree (EDC 10, 30 or 50) and of the initial BMP-2 loaded concentration (20, 60 or 100 μg/mL). The initial (Γ_i) and final (Γ_f) BMP-2 amounts adsorbed on the FS membranes as well as the % of BMP-2 released over the total time period are given. NA: not applicable.

$[BMP\text{-}2]_{initial}$ (μg /ml)	20			60			100		
	Γ_i (μg)	Γ_f (μg)	% Releas	Γ_i (μg)	Γ_f (μg)	% Releas	Γ_i (μg)	Γ_f (μg)	% Releas
EDC 10	2.7±0.4	1.7±0.3	36.9±10.6	7.4±1.8	5.0±0.2	34.3±7.5	10.8±1.2	8.8±2.3	18.0±3.4
EDC 30	3.0±1.0	2.1±0.3	29.5±4.8	NA	NA	NA	NA	NA	NA
EDC 50	3.9±0.2	3.1±0.3	20.8±2.1	4.4±0.6	3.8±0.6	14.4±2.0	8.0±2.6	7.4±2.3	15.0±1.3